

RESEARCH ARTICLE SUMMARY

QUANTUM OPTICS

Imprinting the quantum statistics of photons on free electrons

Raphael Dahan[†], Alexey Gorlach[†], Urs Haeusler[†], Aviv Karnieli[†], Ori Eyal, Peyman Yousefi, Mordechai Segev, Ady Arie, Gadi Eisenstein, Peter Hommelhoff, Ido Kaminer*

INTRODUCTION: The science of light has undergone two major revolutions over the previous two centuries. The first—by Grimaldi, Huygens, Fresnel, Young, and Maxwell—established light as a wave phenomenon, and the second—by Planck, Einstein, and Glauber—established light as a combined particle-wave quantum phenomenon. Despite the quantum revolution, entire areas of science still find the classical wave description of light sufficient, especially so for interactions between light and charged particles such as free electrons. Light and all forms of electromagnetic fields remain pure wave phenomena at the frontiers of free-electron physics, microscopy, accelerators, and radiation sources. We present experiment and theory in which the quantum nature of light plays the key role in its interaction with free electrons.

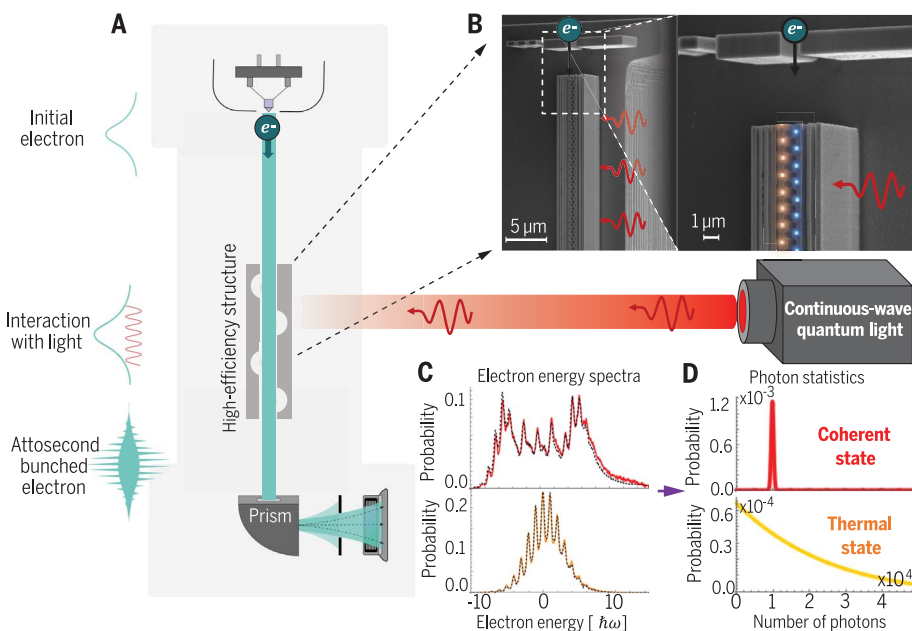
RATIONALE: From the viewpoint of quantum optics, the wave theory of light is sufficient to model its interaction with matter, provided that light and matter do not become entangled during their interaction. This wave description was justified thus far because classical light can be described as coherent states, which stay approximately unchanged under interactions and thus do not become entangled.

Our work demonstrates the interaction of free electrons with light of nontrivial quantum photon statistics. The electron evolves into an entangled joint state with the photons, imprinting their quantum statistics on the electron energy spectrum. By measuring the electron spectrum, we extracted the quantum photon statistics of light, finding the second-order photon correlations $g^{(2)}(0)$ and higher-order correlations $g^{(n)}(0)$. We

demonstrate quantitative measurement of different photon statistics using an optical amplifier operated in different amplification regimes, showing transition from Poissonian statistics in deep saturation to super-Poissonian statistics due to amplified spontaneous emission and eventually a thermal state with Bose-Einstein statistics. Electrons can perform nondestructive quantum measurements, inspiring possibilities in quantum optics such as ultrafast free-electron—based quantum tomography of light at deep suboptical wavelength resolution.

RESULTS: The interacting electron in our experiment acts as a “walker,” performing a quantum/classical walk on the ladder of energy levels, each step corresponding to single-photon emission or absorption. When light interacts as a wave (coherent state, Poissonian statistics), the resulting electron dynamics is also that of a wave—quantum walk, in which a well-defined phase is maintained between the electron energy states. By contrast, when the particle-nature of light becomes dominant (super-Poissonian statistics), the resulting electron dynamics is also that of a particle—classical random walk, in which collapse washes out the relative phase between the electron energy states. This emergence of classical random walk represents a manifestation of Bohr’s correspondence principle between classical and quantum physics—one of the cornerstones of quantum mechanics since its earliest days.

CONCLUSION: We overcame the challenge of the usually weak coupling between light and free electrons by exploiting an inverse design silicon-photonics nanostructure that combines two critical ingredients: photonic cavities and phase-matching between electron wave functions and light waves. Our integrated solution can equip state-of-the-art microscopes with capabilities for temporal electron wave modulation by using continuous-wave (CW) lasers, paving the way toward microscopes operating at simultaneous subangstrom-spatial and few-attosecond-temporal resolution. Coherent temporal modulation of electron wave functions opens possibilities for electron microscopy of phenomena that cannot be explored by other means: imaging nonequilibrium quantum states of matter, measuring their coherence properties and decoherence rates. ■



Quantum optics with free electrons. A silicon-photonics device integrated in an electron microscope provides efficient electron interactions with CW light, enabling the detection of the quantum photon statistics. **(A)** CW modulation of electron wave functions in transmission electron microscopy. **(B)** Highly efficient electron-light interaction facilitated by an inverse-designed silicon-photonics nanostructure (scanning electron microscope image), consisting of a Bragg mirror and a periodic channel that achieves quasi-phase-matching of electron and quantum light. **(C)** The electron energy spectrum after the interaction with two types of light states: coherent and thermal. **(D)** The corresponding photon statistics reconstructed from the measured spectra.

The list of author affiliations is available in the full article online.

*Corresponding author. Email: kaminer@technion.ac.il

[†]These authors contributed equally to this work.

Cite this article as R. Dahan *et al.*, *Science* **373**, eabj7128 (2021). DOI: 10.1126/science.abj7128

S READ THE FULL ARTICLE AT
<https://doi.org/10.1126/science.abj7128>

RESEARCH ARTICLE

QUANTUM OPTICS

Imprinting the quantum statistics of photons on free electrons

Raphael Dahan^{1,2,†}, Alexey Gorlach^{1,2,†}, Urs Haeusler^{3,†,‡}, Aviv Karnieli^{1,2,4,†}, Ori Eyal^{1,2}, Peyman Yousefi^{3,§}, Mordechai Segev^{1,2,5}, Ady Arie⁶, Gadi Eisenstein^{1,2}, Peter Hommelhoff³, Ido Kaminer^{1,2,*}

The interaction between free electrons and light stands at the base of both classical and quantum physics, with applications in free-electron acceleration, radiation sources, and electron microscopy. Yet to this day, all experiments involving free-electron–light interactions are fully explained by describing the light as a classical wave. We observed quantum statistics effects of photons on free-electron–light interactions. We demonstrate interactions that pass continuously from Poissonian to super-Poissonian and up to thermal statistics, revealing a transition from quantum walk to classical random walk on the free-electron energy ladder. The electron walker serves as the probe in nondestructive quantum detection, measuring the second-order photon-correlation $g^{(2)}(0)$ and higher-orders $g^{(n)}(0)$. Unlike conventional quantum-optical detectors, the electron can perform both quantum weak measurements and projective measurements by evolving into an entangled joint state with the photons. These findings inspire hitherto inaccessible concepts in quantum optics, including free-electron–based ultrafast quantum tomography of light.

Understanding of light as a wave phenomenon was firmly established in the early days of the 19th century, forming the foundations of Maxwell's equations (1), the entirety of electrodynamics, and the study of light-matter interactions. Later discoveries revealed the quantum-particle nature of light: starting from the photoelectric (2) to the discovery of entanglement many decades later (3), constituting modern quantum optics (4, 5). Yet, entire areas of science still find the wave description of light fully sufficient. This is true for light in the optical range and for all other forms of electromagnetic waves. For example, classical electromagnetic waves determine the dynamics of charged particles in numerous applications, from free-electron lasers and synchrotrons to radars, communication satellites, and even microwave ovens. Light remains purely a wave phenomenon also at the frontier of free-electron–light

experiments, in which laser-driven electron acceleration [specifically, wakefield accelerators (6, 7) and dielectric laser accelerators (8–12)] still consider the particle motion by using a wave description of the laser. Thus far, the quantum-particle nature of light in its interactions with free electrons has remained hidden, without any direct consequences. This is in sharp contrast to the quantum nature of the electron, which is now regularly observed in ultrafast transmission electron microscopy (13–16). The critical role of the electron quantum wave function in its interaction with light is already well understood (17–22): The electron exchanges integer multiples of the photon energy, as shown in the theoretical description of the technique called photon-induced near-field electron microscopy (PINEM) (13, 17, 18). However, even in this case—in which the electron must be treated quantum-mechanically—the description of light as a classical wave was sufficient in all experiments to date.

Here, we present experiments showing that quantum statistics of photons alter their interaction with free electrons; we demonstrate free-electron–light interactions that cannot be described by treating light as a wave phenomenon. Moreover, we used the electron–light interaction to measure the photon statistics of the light. This capability stems from a fundamental aspect of quantum optics: The interaction with light can create entanglement between the light and the interacting object. Consequently, the joint free-electron–light state becomes a nonseparable state from which we can extract the photon statistics by measuring the electron energy spectrum. Our experiment

demonstrates this concept on amplified light, exhibiting different photon statistics for varying amplification regimes. The free-electron interaction enables us to characterize the amplifier output, showing its transition from a coherent state with Poissonian statistics in the regime of deep saturation to super-Poissonian statistics owing to amplified spontaneous emission and eventually to a thermal state with Bose-Einstein statistics. Our experiments offer a pathway for using free electrons for quantum-state tomography of light, with high resolution in both time and frequency (23).

Bohr's correspondence principle: From free-electron quantum walk to random walk

Our experiment shows that the measured electron acts as a “walker” performing a generalized quantum/classical walk (Fig. 1) on the ladder of energy levels (separated by the single-photon energy $\hbar\omega$), similar to an upside-down (quantum) Galton board experiment (Fig. 1A). At each infinitesimal step, the electron walker either remains in its current energy level, moves to a lower energy level by emitting a photon, or moves to a higher energy level by absorbing a photon. Each step either maintains a well-defined phase between the electron energy states, such as in interactions with a coherent state of light (Fig. 1, left), or washes out the phase and acts in a random fashion, such as in interactions with thermal light (Fig. 1, right). We observed the walk dynamics by measuring the electron energy spectrum as a function of illumination power for different photon statistics (Fig. 1, C and D). The measurement shows that when light interacts as a wave (coherent state), the resulting electron dynamics is also that of a wave—a pure quantum walk. By contrast, when the particle-nature of light becomes dominant (super-Poissonian and thermal statistics), the resulting electron dynamics is also that of a particle—a classical random walk. This emergence of the classical dynamics of random walk from the interaction of a free electron with super-Poissonian light represents a new manifestation of the correspondence principle between classical and quantum physics, which has been one of the cornerstones of quantum mechanics since its earliest days (24).

We begin by formulating the theory of light–free-electron interaction and its dependence on photon statistics. The theory, henceforth called the electron walker theory (explained in Fig. 1, A and B), captures the entire range of experimental parameters, including both limiting cases of coherent and thermal states of light: For the interaction with coherent-state light (Fig. 1, left), the electron undergoes pure quantum walk in energy-space [as shown in (14)], and for the interaction with thermal light (Fig. 1, right), the electron undergoes pure random walk. The intermediate cases of interactions

¹Department of Electrical Engineering, Russell Berrie Nanotechnology Institute, Technion–Israel Institute of Technology, Haifa 32000, Israel. ²Solid State Institute, Technion–Israel Institute of Technology, Haifa 32000, Israel.

³Department of Physics, Friedrich-Alexander-Universität Erlangen-Nürnberg (FAU), Staudtstraße 1, Erlangen 91058, Germany. ⁴Raymond and Beverly Sackler School of Physics and Astronomy, Tel Aviv University, Tel Aviv 69978, Israel.

⁵Department of Physics, Technion–Israel Institute of Technology, Haifa 32000, Israel. ⁶School of Electrical Engineering, Fleischman Faculty of Engineering, Tel Aviv University, Tel Aviv 69978, Israel.

*Corresponding author. Email: kaminer@technion.ac.il

†These authors contributed equally to this work.

‡Present address: Cavendish Laboratory, University of Cambridge, JJ Thomson Avenue, Cambridge CB3 0HE, UK.

§Present address: Fraunhofer-Institut für Keramische Technologien und Systeme IKTS, Aüssere Nürnberger Strasse 62, Forchheim 91301, Germany.

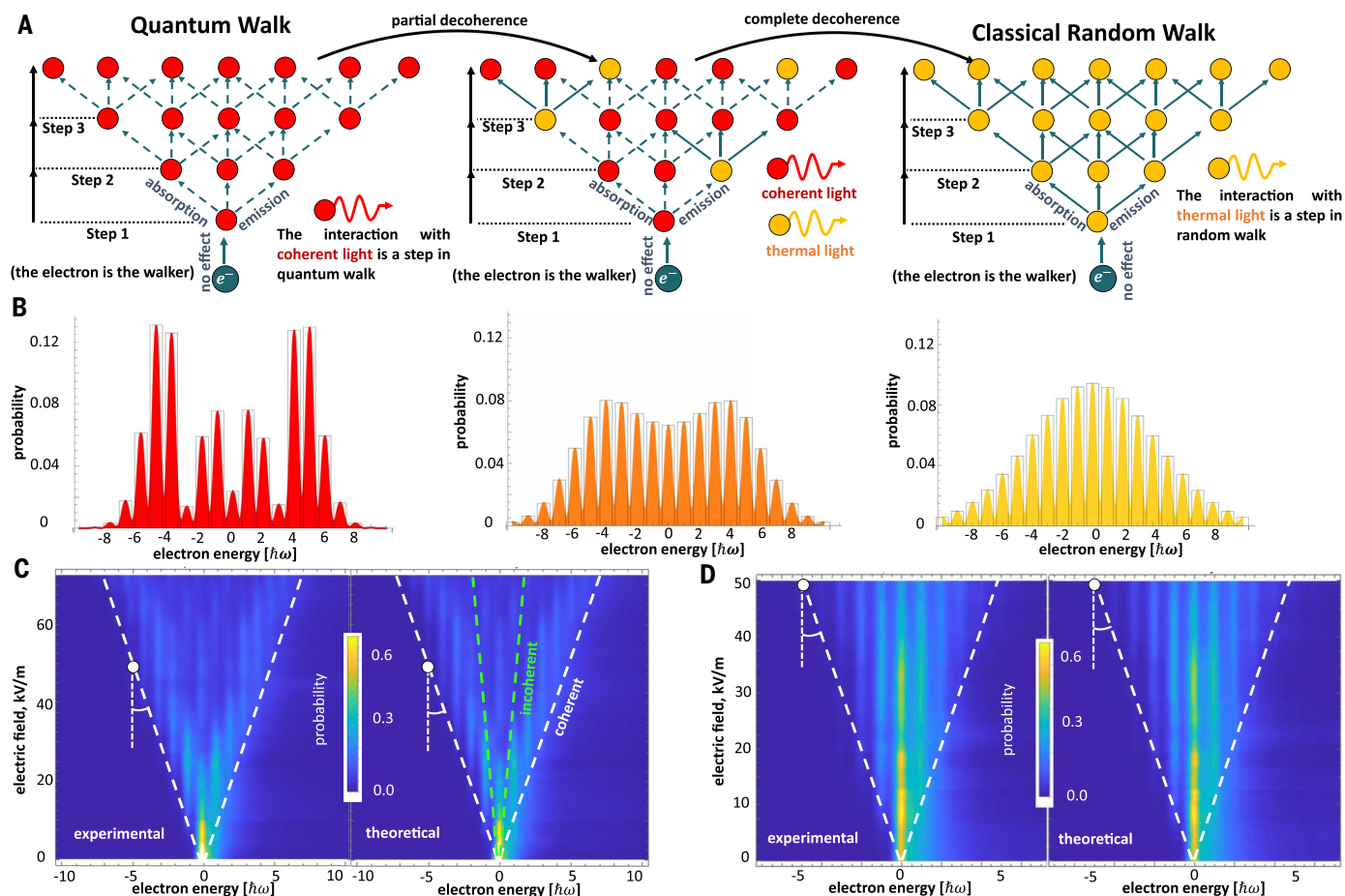


Fig. 1. Free-electron-light interactions imprint the quantum photon statistics on the electron energy spectra, demonstrating the transition from quantum walk to classical random walk of a free electron. (A) The electron walker performs consecutive interactions with the photons. At each infinitesimal step, there are three possibilities: (i) the electron remains in its current energy level; (ii) the electron emits a photon, moving to a lower energy level; or (iii) the electron absorbs a photon, moving to a higher energy level. Each such emission or absorption either maintains a well-defined phase between the electron energy states, as in interactions with coherent-state light (red), or “collapses” and acts in a random fashion, as in interactions with thermal light (yellow). The collapse washes out the phase between the electron energy states. The transition from quantum walk to random walk is expressed by the continuous transition in the photon statistics from Poissonian (coherent state) to super-Poissonian and all the way to a thermal light state. (B) The electron walker theory exactly matches with the Q-PINEM theory, in which the shape of the photon statistics determines the degree of decoherence of the electron. The resulting electron energy spectra show either quantum walk, random walk, or an intermediate case displaying partial decoherence, depending on the photon statistics (a measurement of the continuous transition is provided in Fig. 3). (C and D) Electron

energy spectra for coherent and thermal states evolving with the electric field amplitude. Theory gives an excellent agreement with experimental results, measured in the setup presented in Fig. 2, with more data shown in fig. S13. The white circles indicate that the observed electron energy width is the same for the same driving light intensity, regardless of the quantum statistics. This comparison reveals that the electron interactions with thermal states are as efficient as interactions with coherent states. In (C), we indicate with green dashed lines the electron energy width for light with partial optical coherence (spatial coherence length of $1 \mu\text{m}$; calculation with other values are shown in fig. S16), predicting a different slope than for the measured data that corresponds to light with full optical coherence, indicated with white lines in (C) and (D). Thus, we conclude that the measurements in (D) cannot be explained by a short optical coherence length (further discussion and results are in supplementary text S6 and fig. S16). This shows that the interaction of super-Poissonian light with a free electron does not cause the electron to decohere in time or space. Rather, the electron remains in a coherent superposition of energy states that become more entangled with the light for stronger super-Poissonian statistics, with maximum entanglement for thermal light. The electron energy axis here and in all figures refers to energy loss, as is conventional in electron energy loss spectroscopy.

with super-Poissonian light all correspond to mixtures of quantum walk and random walk, showing a continuous transition between the two phenomena. We show in supplementary text S1 that despite its simplicity, the walker theory provides the same results as those of the quantum-optical generalization of PINEM (Q-PINEM), proposed theoretically in (25, 26) [in particular, Fig. 1D precisely matches the prediction in (26)]. The comparisons in Fig. 1,

C and D, show that the theories successfully describe the measured electron energy spectra, the experimental details of which we describe below.

The agreement of both walker and Q-PINEM theories with the experimental data in Fig. 1, C and D, allows us to draw decisive conclusions about the role of quantum decoherence in the interaction. The photon statistics directly determine the degree of decoherence of the elec-

tron walker: Broader photon distributions (such as super-Poissonian) increase the free-electron decoherence in energy (27) during the electron walk. The limit of thermal light can be understood exactly as the complete decoherence of the electron quantum state at every step of the walk, showing the emergence of classical random walk from the decoherence of quantum walk. The phenomenon of quantum walk has been observed experimentally in a wide range of

physical systems (28–33). In our experiment, there is a fundamental difference: the quantum-to-classical transition of the electron walker we observed arises from the photon distribution rather than from dephasing and disorder-induced decoherence as in many other systems (30, 33–37).

Experimental setup: High-efficiency silicon-photonic electron-light coupler

Our experiment achieved an efficient electron-light interaction by use of two critical ingredients: photonic cavities (38, 39) and phase-matching between the electron wave function and the light wave (40), inspired by phase-matching of classical electron-light interactions (41). We used quasi-phase-matching in custom-made silicon-photonic nanostructures to create efficient free-electron-quantum-light interactions inside a transmission electron microscope (TEM) (Fig. 2A). Our nanostructures are inspired by miniaturized electron accelerators (8–11), which were recently used in a silicon photonics PINEM experiment (12). We used photonic inverse de-

sign methods to design and optimize a high-efficiency electron-light coupler (Fig. 2D) (11, 42), operating at a wavelength of 1064 nm and electron kinetic energy of 189 keV (Fig. 2). The quantum statistics of the output light is modified by controlling the input power to a fiber amplifier and then coupling the light into the nanostructure inside the TEM by using two cylindrical lenses (supplementary materials, materials and methods).

Our experiment realizes strong electron-light interactions; each electron exchanges multiple photons with the light field. Such strong interactions were previously only realized with intense laser pulses synchronized with photoemitted free electrons (8–15, 38–40, 43). In contrast with such intense laser pulses that can be considered as coherent states (classical waves), all other states of light are usually not so intense. The low intensity poses a challenge for investigating their interactions with free electrons. We thus developed nanostructures for enhancing the interaction efficiency, reach-

ing the desired strong electron-light interaction with lower-intensity light, which is especially important for quantum light. The interaction efficiency is high enough to enable the use of continuous-wave (CW) light while still maintaining the strong interaction. Recent experimental works have shown that even weak CW electron-light interactions (up to one photon absorbed or emitted by the electron) have intriguing applications (44–47). Our experiment offers an avenue for taking these ideas forward to regimes of stronger interactions with CW light and specifically enables us to probe the quantum statistics of the photons.

Free-electron-quantum-light interactions

In all free-electron experiments to date, the electron dynamics has been accurately captured by its interaction with classical electromagnetic fields. The dynamics of a single-electron wave function has been fully described by the time-dependent Schrödinger equation (or the Dirac equation in the more general relativistic

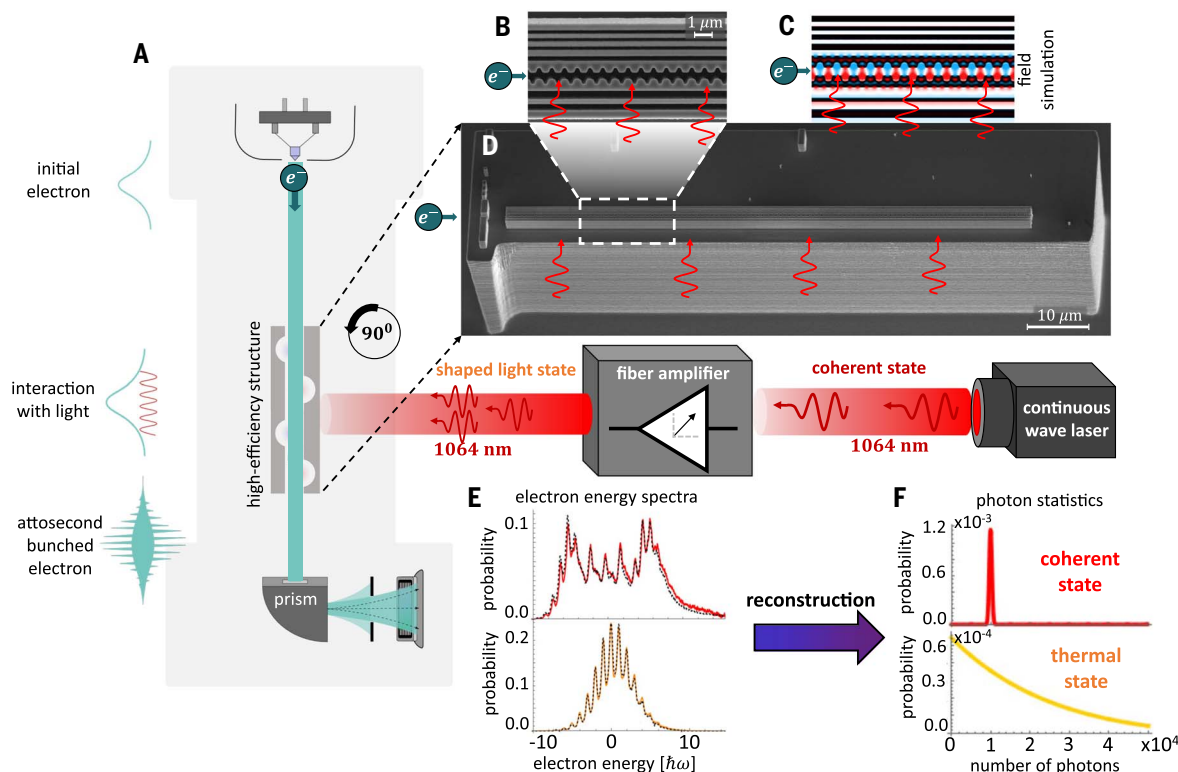


Fig. 2. Free electron interaction with light of different photon statistics in a high-efficiency silicon-photonic nanostructure. (A) We used a high-efficiency electron-light coupler in a transmission electron microscope (TEM) to facilitate efficient interaction of free electrons with CW light. With this, we observed the effect of photon statistics in electron-light interactions. The electron energy spectrum was measured with an energy resolution better than that of the single-photon energy, using EELS. The photon statistics is varied continuously with the fiber amplifier from Poissonian to super-Poissonian and up to thermal. (B) Scanning electron microscope image of the coupling structure. Light and electrons are efficiently coupled by using a resonating quasi-phase-matched structure consisting of a periodic channel and a Bragg mirror. (C) Simulation of

the longitudinal quasi-phase-matched electric field in the nanostructure, optimized with photonic inverse design methods for efficient free-electron-light interaction. (D) Image of the entire nanostructure in three dimensions. More information is provided in the supplementary materials, materials and methods, and fig. S1. (E) Electron energy spectra for interactions with coherent and thermal states. The colored curves denote the theory (fit is explained in fig. S13 and supplementary text S4), and dashed black curves denote the experiment, showing almost perfect overlap. (F) The measured electron spectra are used to extract the photon statistics shown here. The slight asymmetry between gain and loss observed in (E) and in Fig. 3D is explained in supplementary text S4.3.

the longitudinal quasi-phase-matched electric field in the nanostructure, optimized with photonic inverse design methods for efficient free-electron-light interaction. (D) Image of the entire nanostructure in three dimensions. More information is provided in the supplementary materials, materials and methods, and fig. S1. (E) Electron energy spectra for interactions with coherent and thermal states. The colored curves denote the theory (fit is explained in fig. S13 and supplementary text S4), and dashed black curves denote the experiment, showing almost perfect overlap. (F) The measured electron spectra are used to extract the photon statistics shown here. The slight asymmetry between gain and loss observed in (E) and in Fig. 3D is explained in supplementary text S4.3.

case) with the classical vector \mathbf{A} and scalar V potentials

$$i\hbar\partial_t|\psi\rangle_{\text{el}} = \left[(\mathbf{p} + e\mathbf{A}(t))^2/2m + eV(t) \right] |\psi\rangle_{\text{el}} \quad (1)$$

where $\mathbf{p} = -i\hbar\nabla$ is the momentum operator, e and m are the electron charge and mass, and $|\psi\rangle_{\text{el}}$ denotes the electron quantum state. This description was justified so far because in the quantum picture, classical electromagnetic fields can be described as coherent states $|\alpha\rangle_{\text{ph}}$ (48), and intense coherent states stay approximately unchanged under interactions. Consequently, in a full quantum description, the joint electron-photon state $|\psi\rangle_{\text{el-ph}} \approx |\psi\rangle_{\text{el}} \otimes |\alpha\rangle_{\text{ph}}$ remains separable after the interaction with an intense classical field.

By contrast, for some of the photonic states we considered in this work, the joint electron-photon state after the interaction is nonseparable—that is, entangled (49). This situation cannot be described by the commonly used theoretical analysis of a time-dependent Schrödinger equation with nonquantized potentials (Eq. 1) but requires a quantum-optics theory. Below, we present the formulation of the quantum interaction of light with a highly paraxial free-electron beam—the Q-PINEM theory (23, 25, 26), which has the scattering matrix

$$S = \exp\left(g_q b a^\dagger - g_q^* b^\dagger a\right) \quad (2)$$

where g_q is the quantum coupling constant; a and a^\dagger are the photonic annihilation and creation operators, respectively; and b and b^\dagger are the free-electron energy ladder operators describing the electron losing or gaining a single-photon energy quantum, respectively. The resulting joint electron-photon state is generally nonseparable, and its density matrix can be written as

$$\rho_{\text{el-ph}} = \sum_{n,m=0}^{\infty} \rho_{\text{ph}}(n,m) |\psi^n\rangle_{\text{el-ph}} \langle\psi^m|_{\text{el-ph}} \quad (3)$$

where $\rho_{\text{ph}}(n,m) = \langle n|\rho_{\text{ph}}|m\rangle$ is the density matrix element of the light in Fock space. Each pure-state component $|\psi^n\rangle_{\text{el-ph}}$ is a superposition of electron-photon product states. The experimental conditions allow us to consider the initial electron as a single-energy state $|E_0\rangle_{\text{el}}$ with energy uncertainty smaller than the energy $\hbar\omega$ of a single photon of the field with which it interacts. In this case, we can express the joint electron-photon state as

$$|\psi^n\rangle_{\text{el-ph}} = \sum_{k=-\infty}^{\infty} c_k^n |E_0 - k\hbar\omega\rangle_{\text{el}} \otimes |n+k\rangle_{\text{ph}} \quad (4)$$

where $|n+k\rangle_{\text{ph}}$ is a Fock state of light with $n+k$ photons, and $|E_0 - k\hbar\omega\rangle_{\text{el}}$ is the electron

state with energy $E_0 - k\hbar\omega$. Equation 4 shows that the free-electron-light interaction can create nonseparable quantum states. By solving Eq. 2 for the state evolution, we find the coefficients $c_k^n = |g_q|^{-1} (-1)^n e^{i\phi_g k} W_{n+\frac{1}{2}(k+1), \frac{1}{2}|k|}(|g_q|^2) / \sqrt{(n+k)!n!}$, where W is the Whittaker function and ϕ_g is the phase of g_q (supplementary text S2). In the limit of weak interaction and a large number of photons, the coefficients become $c_k^n \approx e^{i\phi_g k} J_k(2|g_q|\sqrt{n})$ (23, 26), which is reminiscent of the PINEM theory (17, 18).

Extracting the photon statistics from the electron energy spectrum

The photon statistics encapsulated in the photonic density matrix ρ_{ph} can dramatically change the measured electron energy spectrum (23, 25, 26). We used this concept to experimentally demonstrate how the statistics of light interacting with free electrons is imprinted on the corresponding electron energy spectra. The probability P_k to measure an electron energy shifted by k photons depends on ρ_{ph} through $P_k = \sum_n |c_{-k}^{n+k}|^2 \rho_{\text{ph}}(n+k, n+k)$. By inverting this relation, we can extract the photon statistics from the measured electron energy spectrum (Fig. 3). Specifically, five electron energy spectra (experiment and theory, respectively) are shown in Fig. 3, A and B, throughout the continuous transition between amplified spontaneous emission and amplified coherent-state of light; the extracted photon statistics for each case are shown in Fig. 3C.

To unveil the role of photon statistics, the state of light (Fig. 3A) was gradually varied from coherent to thermal, and the statistics were reconstructed at each stage (Fig. 3C). The statistics were determined by varying the power of a laser beam seeding the fiber amplifier, varying the gain saturation and output power (50, 51). The optical power entering the electron microscope was kept constant by using an attenuator. This way, the photon statistics can be changed without changing the average number of photons (Fig. 3F). Therefore, the measurement in Fig. 3A directly corresponds to the quantum-to-classical transition of the free-electron quantum/classical walk shown in Fig. 1, A and B. As explained in supplementary text S4.4 and fig. S16, our observations cannot arise from the lack of spatial or temporal optical coherence nor from spatial or temporal inhomogeneity of the light driving the interaction.

To clarify, the term “coherence” is used in two different contexts: (i) The classical optical coherence is characterized by spatial coherence lengths and temporal coherence duration. All types of light in our experiment have the same optical coherence during the interaction with the electron (supplementary text S6). (ii) The quantum coherence relates to the quantum photon statistics and is defined by the corre-

lations $g^{(n)}$. Specifically, $g^{(2)}$ is different for coherent and thermal states. Here, in the context of quantum optics, the term “coherent” also appears as the name of the “coherent state” as defined by Glauber (52). In this sense, the thermal light is incoherent (given by a diagonal density matrix). This notion of coherence generalizes the classical optical coherence, which is given as the special case of $g^{(1)}$. The effect of quantum coherence is what we studied in our experiment.

The limiting case of a coherent state corresponds to an approximately separable $\rho_{\text{el-ph}}$, whereas the other limiting case of a thermal state corresponds to a nonseparable $\rho_{\text{el-ph}}$. This can be directly seen in Eq. 3, where ρ_{ph} of thermal light is diagonal, making the joint $\rho_{\text{el-ph}}$ nonseparable. Both limiting cases, and all cases in between, can be accurately captured by the Q-PINEM theory (Eqs. 2 to 4). To quantify the quantum-optical state of light, the corresponding second-order degree of coherence $g^{(2)}(0)$ was extracted from each electron spectrum (Fig. 3F), as first proposed in (26). Moreover, because the entire photon distribution can be extracted (Fig. 3C), it directly provides all the photon-number moments $\langle n^m \rangle$ (23) and thus also the higher-order $g^{(n)}(0)$ (26).

The ability to control and measure the photon statistics during light-free-electron interaction offers a variety of applications. As a proof-of-concept application, we characterize the amplifier output when it undergoes a transition from the limit of Poissonian statistics in the regime of deep saturation to super-Poissonian statistics created by amplified spontaneous emission (5). The amplifier has a coherent input seed of amplitude α and a saturable gain $\mathcal{G} = \mathcal{G}(|\alpha|^2)$, generating light with the following photon statistics (supplementary text S3):

$$\rho_{\text{ph}}(n,n) = e^{-|\alpha|^2} \frac{1}{\mathcal{G}} \left(1 - \frac{1}{\mathcal{G}}\right)^n L_n\left(-\frac{|\alpha|^2}{\mathcal{G}-1}\right) \quad (5)$$

where $L_n(x)$ is the n th Laguerre polynomial. By tuning α and \mathcal{G} , the photon statistics of the output light can be continuously tuned between amplified coherent state (for $|\alpha| \gg 1$ saturated \mathcal{G} , approaching a Poissonian photon distribution) to thermal amplified spontaneous emission (for $|\alpha| \approx 0$ linear $\mathcal{G} \gg 1$, approaching a thermal photon distribution).

We extracted the amplifier gain curve from the analysis of the electron energy spectrum (fig. S10) and performed two additional independent measurements of the amplifier gain that both show good agreement (fig. S10E), from the optical spectra and from direct power measurements. This comparison supports our estimation of the photon statistics from the amplifier model. Furthermore, the gain curves can be used to estimate the quantum coupling

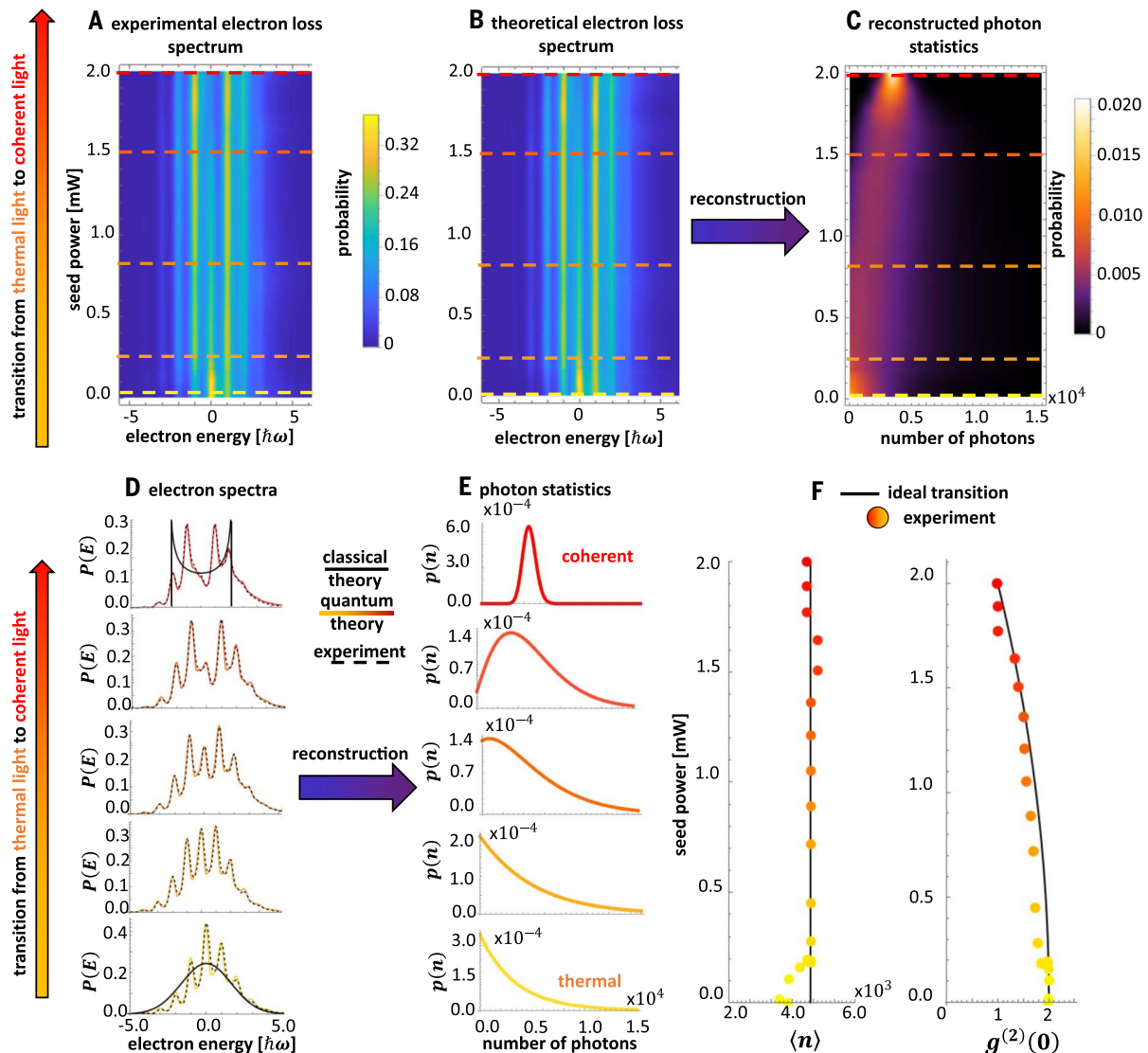


Fig. 3. Experimental reconstruction of photon statistics from electron energy spectra. (A) The measured electron energy spectra for a range of fiber amplifier parameters, showing a continuous transition from coherent Poissonian light in the regime of deep saturation to super-Poissonian and eventually thermal light, created through amplified spontaneous emission. The average photon number is the same in all cases. (B) The corresponding theoretical calculation of the electron spectra is based on the Q-PINEM theory (Eqs. 2 to 4) with the quantum-optical amplifier model (Eq. 5 and supplementary text S3). (C) We reconstructed the photon statistics of light from the experimentally obtained electron spectra (A) by using the fitted parameters of the theoretical model (B) and substituted them in

the amplifier model (supplementary text S4). (D) Selected cases of measured electron energy spectra after the interaction with different states of light. The data (dashed black curve) show an excellent match to the Q-PINEM theory (colored solid curve). By contrast, simulations using a point electron (solid black curve) do not at all agree with the quantum predictions, indicating that the effects cannot be obtained from an incoherent point electron mixture or collapse in time (supplementary text S7). (E) Reconstructed photon statistics corresponding to the selected cases of (D). (F) The average number of photons $\langle n \rangle$ and second-order correlation (degree of coherence) $g^{(2)}(0)$ extracted from the measurements. The black curves correspond to the theory (supplementary text S2) with the same parameters.

constant g_q up to the coupling efficiency of the light to the structure (supplementary text S4). In this fashion, the free-electron quantum-optical detection can be applied to extract the ultrafast quantum statistics emerging from amplifiers operating on subpicosecond and even subfemtosecond time scales.

The free electron as a probe of quantum weak measurement

The free electron can serve as the probe in quantum nondestructive detection of the state

of light ρ_{ph} (53), as suggested theoretically in the context of PINEM (54). The electron plays the role of the measurement device and pointer, and the light plays the role of the system to be measured. Specifically, the electron detection in the electron energy loss spectrometer (EELS) is a strong projective measurement of the electron that can be modeled by a set of projection operators $M_k = |E_0 - k\hbar\omega\rangle\langle E_0 - k\hbar\omega|$. After a projection by M_k , the state of light changes from ρ_{ph} to a new state denoted by ρ_{ph}^k (the superscript k indicates the correlation with

the electron measurement). The density matrix of this light ρ_{ph}^k may or may not differ significantly from the original state ρ_{ph} , depending on the level of entanglement with the electron. The difference is quantified by the fidelity $F_k = \left[\text{tr} \left\{ \sqrt{\sqrt{\rho_{ph}} \rho_{ph}^k \sqrt{\rho_{ph}}} \right\} \right]^2$ (55) between ρ_{ph} and ρ_{ph}^k for each value of k (plotted in Fig. 4A). High fidelity ($F_k \rightarrow 1$) means that the light is mostly unchanged by the measurement, whereas low fidelity ($F_k \rightarrow 0$) means that the light is substantially changed by the measurement.

The electron can act as a probe for weak quantum measurements (56–60) with a near-unity fidelity for interactions with a coherent state of light—that is, the electron performs a measurement of the light yet does not substantially affect the quantum state of the light, which is why the process is a weak quantum measurement. By contrast, the interaction with thermal light causes a substantial reduction in the fidelity, implying that the electron probe acts more like a projective measurement that does alter the state of light. Therefore, the same electron probe manifests both extremes: weak measurement and projective measurement (Fig. 4A), depending on the state of the mea-

sured system. To test this observation, a direct measurement of the outgoing state of light after the interaction could be performed by using high-efficiency coupling into or out of the nanophotonic structure (supplementary text S5.4), which is beyond the scope of this work.

To show theoretically the role of the electron probe in the measurement process, we calculated the purity of the post-interaction electron (Fig. 4B), which shows that the electron maintains a purity of unity for coherent state of light, but the purity substantially decreases for thermal light. Such a substantial reduction in purity can be understood as the “collapse” of the electron wave function in the

energy domain. The walker theory we developed (supplementary text S1) shows that this description accurately captures the measured effect and precisely matches the Q-PINEM theory. Through the walker theory, the electron-light interaction can be understood as consecutive infinitesimal steps at which the electron quantum state partially collapses in energy, with full collapse occurring for a thermal state of light, resulting in a pure random walk, or no collapse occurring for a coherent state of light, resulting in a pure quantum walk. The electron wave function never collapses in time and space but only in the energy domain. Spatially and temporally, the electron remains a

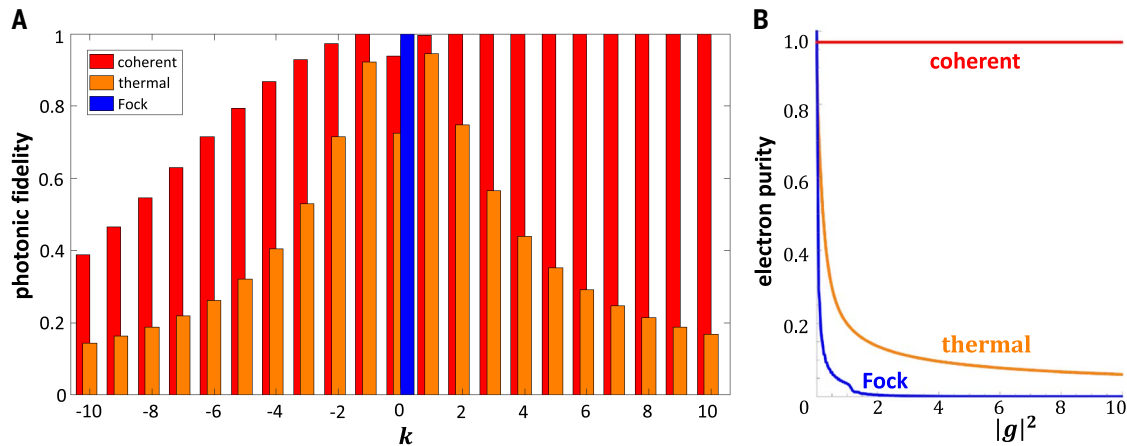


Fig. 4. Photonic fidelity and electron purity after a free-electron-quantum-light interaction. (A) Calculated fidelities between the photonic state before and after its interaction with a free electron, which subsequently undergoes a projective measurement. The fidelity is plotted as a function of the energy state $|E_0 - \hbar\omega k\rangle$ in which the electron is detected. We present the fidelity for different states of light, all with an average photon number $\langle n \rangle = 100$ and quantum coupling $g_q = 0.1$. The fidelity is high for a coherent state, indicating that for small-enough g_q , the electron can serve as a probe of quantum weak measurement. For the thermal state, the fidelity is much lower, indicating a

behavior closer to strong projective measurement. As a comparison, we also present the fidelity for a Fock state, for which the measurement is projective (fidelity of zero) for any $k \neq 0$. The fidelity asymmetry for the coherent case is explained by the fundamental difference between subtracting or adding photons to a coherent state (supplementary text S2). (B) Electron purity after its interaction with different states of light as a function of the classical coupling strength $|g|^2 = |g_q|^2 \langle n \rangle$. The electron stays pure after an interaction with a coherent state, but its purity diminishes much faster for a thermal state, as an indication of emerging entanglement between the electron and light.

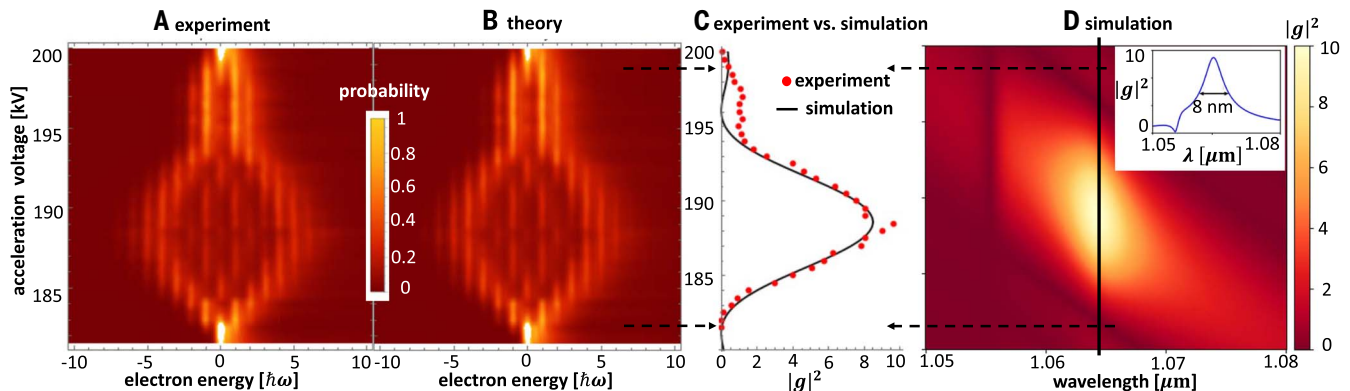


Fig. 5. Measurement of the quasi-phase-matching condition. (A) Electron energy spectra measured for a range of electron kinetic energies, (B) showing a good agreement with theory. (C) The classical interaction strength $|g|^2 = |g_q|^2 \langle n \rangle$ and effective interaction length are extracted from the data by comparing it with the quasi-phase-matching theory (supplementary text S5). (D) Simulation of $|g|^2$ as a function of electron kinetic energy and laser wavelength, showing the resonant nature of the quasi-phase-matched interaction. A version of (D) for a longer structure is provided in fig. S15, allowing a better frequency resolution for isolating a single mode in the structure.

coherent wave function that extends over many cycles of the field, as evident by the emergence of discretized energy peaks (such as in Fig. 3D and in all other figures), occurring even with thermal light. A collapse in time or space, if it ever appears, would manifest as an incoherent mixture of point particles interacting with the light field, which cannot result in discrete energy peaks (Fig. 3D, solid black curves, and supplementary text S7). By contrast, the collapse in energy occurring in our experiment causes the electron to split into multiple extended wave functions, in a joint quantum state entangled with the state of light.

The role of quasi-phase-matching and connection to the Smith-Purcell effect

The key to the efficient electron-light coupling that enables our entire experiment is matching the electron velocity with the phase velocity of light trapped in the nanostructure. This phenomenon is known as quasi-phase-matching between free electrons and light (supplementary text S5), also known as the inverse Smith-Purcell effect (9, 61). Our realization of this effect goes beyond conventional realizations of inverse Smith-Purcell experiments in three ways: (i) using CW light rather than laser pulses; (ii) having an electron wave function rather than a classical point electron, as proposed theoretically in (62–64); and (iii) varying the photon statistics so that the experiment deviates from the semiclassical theory treated in (62, 63) and generally cannot be described by any time-dependent Schrödinger equation (Eq. 1). To highlight and quantify the quasi-phase-matching, we scanned over the electron energy (Fig. 5), searching for the optimal electron-light coupling conditions. The optimal acceleration voltage was found to be 189 keV, and we estimate the effective interaction length to be 56 μm , shorter than the structure length of 84 μm . This deviation arises from the 51- μm full width at half maximum transverse intensity profile of the light beam (supplementary materials, materials and methods).

Discussion and outlook

The underlying quantum-optical theory that describes our experiment is best understood in light of recent theoretical advances (25, 26, 64), which have caused a paradigm shift in how we think about the interaction of free electrons and light. Specifically, these and other works show how the interaction becomes sensitive to the photon statistics (23, 25, 26, 64–67) and provide opportunities for shaping electron wave functions (65). These promising ideas provide new opportunities for research in free-electron quantum optics, suggesting new concepts such as electron-light entanglement that can induce electron-electron entanglement (25, 68, 69). This entanglement can in turn be used to create new quantum light sources (66), improve cathodoluminescence techniques (68, 70), and develop

future Cherenkov detectors for particle physics (71). Because all previous free-electron-light experiments worked with classical (coherent state) light, our experiment is a proof of concept for the predictions on interactions between free electrons and nonclassical light, paving the path for these exciting applications.

On the technical side, our experiment highlights new applications of silicon-photonic nanostructures in the field of quantum optics, in which free electrons provide a mechanism to extract the quantum photon statistics. This concept can be extended into full quantum-state tomography of light (23) by using Ramsey-type experiments (19). This approach to quantum-state tomography does not have to destroy or absorb the measured light. Such free-electron-based quantum-optical detectors can have extremely broad bandwidths and the ability to selectively detect individual modes by using phase-matching (supplementary materials S5). The outlook of such quantum-optical detection techniques depends on the efficient coupling of light into the nanostructure that performs the electron-light interaction; the necessary coupling capabilities are already available as on-chip technology (11, 72).

Our small electron probe (30 nm in diameter) is sensitive to minute transverse changes in the field across the channel of the nanostructure, mapping the field at deep subwavelength resolution. Thus, our methods can help identify optimal operation conditions of these nanostructures for different applications, such as laser-driven electron acceleration. Future experiments would enable comparing performances of different electron accelerators: between the more traditional pillars-based nanostructures (73) and ones based on inverse design optimization (11). We can characterize the spectral response with a resolution limited only by the excitation linewidth, being extremely narrow if using a tunable CW source.

Over the past decade, coherent shaping of spatial electron wave functions (43, 74–78) has opened new avenues in electron microscopy, such as electron magnetic circular dichroism (75) and aberration corrections (79). More recently, coherent temporal modulation of electron wave functions (14, 19, 47, 65, 80, 81) has excited new ideas for ultrafast light-matter interactions and free-electron coherent control (19, 20, 82). Especially interesting are the applications of modulation by CW light, showing better phase contrast (44), PINEM by means of electron post-selection (45), plasmon excitation mapping (46), and advances toward attosecond-resolution metrology (47). However, reaching strong electron modulation in a CW operation has been a longstanding challenge that remained unanswered. Our experimental demonstration paves the way toward

equipping state-of-the-art microscopes with CW silicon-photonic light couplers. The modulation capabilities may be further extended to combined spatial and temporal shaping, with a structured light-electron nanophotonic coupler and/or specially shaped light beams (83). Such dream microscopes could operate at simultaneous subangstrom-spatial and few-attosecond-temporal resolution (19–21, 84) and lead to breakthrough experiments in some of the hardest fundamental problems: providing direct observation of molecular excitation dynamics, electron transport phenomena, transient subcycle phenomena in optical nonlinearities, ultrafast plasma oscillations, and many more effects that cannot be explored by other means.

A related work that also shows CW PINEM by using silicon photonic structures was placed on arXiv in parallel with our work (85).

REFERENCES AND NOTES

- J. C. Maxwell, A dynamical theory of the electromagnetic field. *Philos. Trans. R. Soc. Lond.* **155**, 459–512 (1865). doi: 10.1098/rstl.1865.0008
- A. Einstein, Über einem die Erzeugung und Verwandlung des Lichtes betreffenden heuristischen Gesichtspunkt. *Ann. Phys.* **322**, 132–148 (1905). doi: 10.1002/andp.19053220607
- A. Aspect, P. Grangier, G. Roger, Experimental realization of Einstein-Podolsky-Rosen-Bohm Gedankenexperiment: A new violation of Bell's inequalities. *Phys. Rev. Lett.* **49**, 91–94 (1982). doi: 10.1103/PhysRevLett.49.91
- M. O. Scully, M. S. Zubairy, *Quantum Optics* (Cambridge Univ. Press, 1999).
- R. Loudon, *The Quantum Theory of Light* (Oxford, 2000)
- F. Amiranoff et al., Observation of laser wakefield acceleration of electrons. *Phys. Rev. Lett.* **81**, 995–998 (1998). doi: 10.1103/PhysRevLett.81.995
- T. Tajima, X. Q. Yan, T. Ebisuzaki, Wakefield acceleration. *Rev. Modern Plasma Phys.* **4**, 7 (2020). doi: 10.1007/s41614-020-0043-z
- E. A. Peralta et al., Demonstration of electron acceleration in a laser-driven dielectric microstructure. *Nature* **503**, 91–94 (2013). doi: 10.1038/nature12664; PMID: 24077116
- J. Breuer, P. Hommelhoff, Laser-based acceleration of nonrelativistic electrons at a dielectric structure. *Phys. Rev. Lett.* **111**, 134803 (2013). doi: 10.1103/PhysRevLett.111.134803; PMID: 24116785
- R. J. England et al., Dielectric laser accelerators. *Rev. Mod. Phys.* **86**, 1337–1389 (2014). doi: 10.1103/RevModPhys.86.1337
- N. V. Sapa et al., On-chip integrated laser-driven particle accelerator. *Science* **367**, 79–83 (2020). doi: 10.1126/science.aay5734; PMID: 31896715
- Y. Adiv et al., Observation of the quantum nature of laser-driven particle acceleration. CLEO conference SW46.4. (2020).
- B. Barwick, D. J. Flannigan, A. H. Zewail, Photon-induced near-field electron microscopy. *Nature* **462**, 902–906 (2009). doi: 10.1038/nature08662; PMID: 20016598
- A. Feist et al., Quantum coherent optical phase modulation in an ultrafast transmission electron microscope. *Nature* **521**, 200–203 (2015). doi: 10.1038/nature14463; PMID: 25971512
- L. Piazza et al., Simultaneous observation of the quantization and the interference pattern of a plasmonic near-field. *Nat. Commun.* **6**, 6407 (2015). doi: 10.1038/ncomms7407; PMID: 25728197
- A. Arbouet, G. M. Caruso, F. Houdellier, in *Advances in Imaging and Electron Physics*, P. W. Hawkes, Ed. (Academic Press, 2018), vol. 207, pp. 1–72.
- F. J. Garcia de Abajo, A. Asenjo-Garcia, M. Kociak, Multiphoton absorption and emission by interaction of swift electrons with evanescent light fields. *Nano Lett.* **10**, 1859–1863 (2010). doi: 10.1021/nl100613s; PMID: 20415459
- S. T. Park, M. Lin, A. H. Zewail, Photon-induced near-field electron microscopy (PINEM): Theoretical and experimental. *New J. Phys.* **12**, 123028 (2010). doi: 10.1088/1367-2630/12/12/123028
- K. E. Priebe et al., Attosecond electron pulse trains and quantum state reconstruction in ultrafast transmission electron microscopy. *Nat. Photonics* **11**, 793–797 (2017). doi: 10.1038/s41566-017-0045-8

20. G. M. Vanacore *et al.*, Attosecond coherent control of free-electron wave functions using semi-infinite light fields. *Nat. Commun.* **9**, 2694 (2018). doi: [10.1038/s41467-018-05021-x](https://doi.org/10.1038/s41467-018-05021-x); pmid: [30002367](https://pubmed.ncbi.nlm.nih.gov/30002367/)
21. Y. Morimoto, P. Baum, Diffraction and microscopy with attosecond electron pulse trains. *Nat. Phys.* **14**, 252–256 (2018). doi: [10.1038/s41567-017-0007-6](https://doi.org/10.1038/s41567-017-0007-6)
22. Y. Pan, B. Zhang, A. Gover, Anomalous photon-induced near-field electron microscopy. *Phys. Rev. Lett.* **122**, 183204 (2019). doi: [10.1103/PhysRevLett.122.183204](https://doi.org/10.1103/PhysRevLett.122.183204); pmid: [31144903](https://pubmed.ncbi.nlm.nih.gov/31144903/)
23. A. Gorlach *et al.*, Ultrafast non-destructive measurement of the quantum state of light using free electrons. [arXiv:2012.12069](https://arxiv.org/abs/2012.12069) [quant-ph] (2020).
24. C. Cohen-Tannoudji, B. Diu, F. Laloe, *Quantum Mechanics* (Wiley-Interscience, 2006), vol. 1.
25. O. Kfir, Entanglements of electrons and cavity photons in the strong-coupling regime. *Phys. Rev. Lett.* **123**, 103602 (2019). doi: [10.1103/PhysRevLett.123.103602](https://doi.org/10.1103/PhysRevLett.123.103602); pmid: [31573279](https://pubmed.ncbi.nlm.nih.gov/31573279/)
26. V. di Giulio, M. Kociak, F. J. G. de Abajo, Probing quantum optical excitations with fast electrons. *Optica* **6**, 1524–1534 (2019). doi: [10.1364/OPTICA.6.001524](https://doi.org/10.1364/OPTICA.6.001524)
27. Analogously, although unrelated to quantum walks, broader photon distributions also lead to increased decoherence in other quantum systems, such as Rabi oscillations (86).
28. C. A. Ryan, M. Laforest, J. C. Boileau, R. Laflamme, Experimental implementation of a discrete-time quantum random walk on an NMR quantum-information processor. *Phys. Rev. A* **72**, 062317 (2005). doi: [10.1103/PhysRevA.72.062317](https://doi.org/10.1103/PhysRevA.72.062317)
29. H. B. Perets *et al.*, Realization of quantum walks with negligible decoherence in waveguide lattices. *Phys. Rev. Lett.* **100**, 170506 (2008). doi: [10.1103/PhysRevLett.100.170506](https://doi.org/10.1103/PhysRevLett.100.170506); pmid: [18518267](https://pubmed.ncbi.nlm.nih.gov/18518267/)
30. M. Karski *et al.*, Quantum walk in position space with single optically trapped atoms. *Science* **325**, 174–177 (2009). doi: [10.1126/science.1174436](https://doi.org/10.1126/science.1174436); pmid: [19589996](https://pubmed.ncbi.nlm.nih.gov/19589996/)
31. F. Zähringer *et al.*, Realization of a quantum walk with one and two trapped ions. *Phys. Rev. Lett.* **104**, 100503 (2010). doi: [10.1103/PhysRevLett.104.100503](https://doi.org/10.1103/PhysRevLett.104.100503); pmid: [20366407](https://pubmed.ncbi.nlm.nih.gov/20366407/)
32. P. M. Preiss *et al.*, Strongly correlated quantum walks in optical lattices. *Science* **347**, 1229–1233 (2015). doi: [10.1126/science.1260364](https://doi.org/10.1126/science.1260364); pmid: [25766229](https://pubmed.ncbi.nlm.nih.gov/25766229/)
33. S. Dadrás, A. Gresch, C. Groiseau, S. Wimberger, G. S. Summy, Quantum walk in momentum space with a Bose-Einstein condensate. *Phys. Rev. Lett.* **121**, 070402 (2018). doi: [10.1103/PhysRevLett.121.070402](https://doi.org/10.1103/PhysRevLett.121.070402); pmid: [30169047](https://pubmed.ncbi.nlm.nih.gov/30169047/)
34. V. Kendon, Decoherence in quantum walks—A review. *Math. Structures Comput. Sci.* **17**, 1169–1220 (2007). doi: [10.1017/S0960129507006354](https://doi.org/10.1017/S0960129507006354)
35. M. A. Broome *et al.*, Discrete single-photon quantum walks with tunable decoherence. *Phys. Rev. Lett.* **104**, 153602 (2010). doi: [10.1103/PhysRevLett.104.153602](https://doi.org/10.1103/PhysRevLett.104.153602); pmid: [20481989](https://pubmed.ncbi.nlm.nih.gov/20481989/)
36. A. Schreiber *et al.*, Decoherence and disorder in quantum walks: From ballistic spread to localization. *Phys. Rev. Lett.* **106**, 180403 (2011). doi: [10.1103/PhysRevLett.106.180403](https://doi.org/10.1103/PhysRevLett.106.180403); pmid: [21635071](https://pubmed.ncbi.nlm.nih.gov/21635071/)
37. N. C. Harris *et al.*, Quantum transport simulations in a programmable nanophotonic processor. *Nat. Photonics* **11**, 447–452 (2017). doi: [10.1038/nphoton.2017.95](https://doi.org/10.1038/nphoton.2017.95)
38. K. Wang *et al.*, Coherent interaction between free electrons and a photonic cavity. *Nature* **582**, 50–54 (2020). doi: [10.1038/s41586-020-2321-x](https://doi.org/10.1038/s41586-020-2321-x); pmid: [32494081](https://pubmed.ncbi.nlm.nih.gov/32494081/)
39. O. Kfir *et al.*, Controlling free electrons with optical whispering-gallery modes. *Nature* **582**, 46–49 (2020). doi: [10.1038/s41586-020-2320-y](https://doi.org/10.1038/s41586-020-2320-y); pmid: [32494079](https://pubmed.ncbi.nlm.nih.gov/32494079/)
40. R. Dahan *et al.*, Resonant phase-matching between a light wave and a free-electron wave function. *Nat. Phys.* **16**, 1123–1131 (2020). doi: [10.1038/s41567-020-01042-w](https://doi.org/10.1038/s41567-020-01042-w)
41. M. Kozák *et al.*, Acceleration of sub-relativistic electrons with an evanescent optical wave at a planar interface. *Opt. Express* **25**, 19195–19204 (2017). doi: [10.1364/OE.25.019195](https://doi.org/10.1364/OE.25.019195); pmid: [29041113](https://pubmed.ncbi.nlm.nih.gov/29041113/)
42. T. W. Hughes, I. A. D. Williamson, M. Minkov, S. Fan, Forward-mode differentiation of Maxwell's equations. *ACS Photonics* **6**, 3010–3016 (2019). doi: [10.1021/acsp Photonics.9b01238](https://doi.org/10.1021/acsp Photonics.9b01238)
43. G. M. Vanacore *et al.*, Ultrafast generation and control of an electron vortex beam via chiral plasmonic near fields. *Nat. Mater.* **18**, 573–579 (2019). doi: [10.1038/s41563-019-0336-1](https://doi.org/10.1038/s41563-019-0336-1); pmid: [31061485](https://pubmed.ncbi.nlm.nih.gov/31061485/)
44. O. Schwartz *et al.*, Laser phase plate for transmission electron microscopy. *Nat. Methods* **16**, 1016–1020 (2019). doi: [10.1038/s41592-019-0552-2](https://doi.org/10.1038/s41592-019-0552-2); pmid: [31562475](https://pubmed.ncbi.nlm.nih.gov/31562475/)
45. P. Das *et al.*, Stimulated electron energy loss and gain in an electron microscope without a pulsed electron gun. *Ultramicroscopy* **203**, 44–51 (2019). doi: [10.1016/j.ultramicro.2018.12.011](https://doi.org/10.1016/j.ultramicro.2018.12.011); pmid: [31000482](https://pubmed.ncbi.nlm.nih.gov/31000482/)
46. C. Liu *et al.*, Continuous wave resonant photon stimulated electron energy-gain and electron energy-loss spectroscopy of individual plasmonic nanoparticles. *ACS Photonics* **6**, 2499–2508 (2019). doi: [10.1021/acsp Photonics.9b00830](https://doi.org/10.1021/acsp Photonics.9b00830)
47. A. Ryabov, J. W. Thurner, D. Nabben, M. V. Tsarev, P. Baum, Attosecond metrology in a continuous-beam transmission electron microscope. *Sci. Adv.* **6**, eabb1393 (2020). doi: [10.1126/sciadv.abb1393](https://doi.org/10.1126/sciadv.abb1393); pmid: [33177078](https://pubmed.ncbi.nlm.nih.gov/33177078/)
48. The coherent state $|\alpha\rangle_{ph}$, electric field phasor $E_e(z)$, and time-dependent potential $\mathbf{A}(t)$ all describe the same electromagnetic field throughout the paper (64).
49. The nonseparable electron-photon quantum state can also involve nonlocality, once the electron and photons propagate away from the interaction area.
50. M. Shtaiif, G. Eisenstein, Experimental study of the statistical properties of nonlinearly amplified signals in semiconductor optical amplifiers. *IEEE Photonics Technol. Lett.* **9**, 904–906 (1997). doi: [10.1109/68.593341](https://doi.org/10.1109/68.593341)
51. M. Shtaiif, B. Tromborg, G. Eisenstein, Noise spectra of semiconductor optical amplifiers: Relation between semiclassical and quantum descriptions. *IEEE J. Quantum Electron.* **34**, 869–878 (1998). doi: [10.1109/3.668775](https://doi.org/10.1109/3.668775)
52. R. J. Glauber, Nobel Lecture: One hundred years of light quanta. *Rev. Mod. Phys.* **78**, 1267–1278 (2006). doi: [10.1103/RevModPhys.78.1267](https://doi.org/10.1103/RevModPhys.78.1267); pmid: [16888746](https://pubmed.ncbi.nlm.nih.gov/16888746/)
53. A. Reiserer, S. Ritter, G. Rempe, Nondestructive detection of an optical photon. *Science* **342**, 1349–1351 (2013). doi: [10.1126/science.1246164](https://doi.org/10.1126/science.1246164); pmid: [24231809](https://pubmed.ncbi.nlm.nih.gov/24231809/)
54. Y. Pan *et al.*, Weak measurement, projective measurement and quantum-to-classical transitions in electron-photon interactions. [arXiv:1910.11685](https://arxiv.org/abs/1910.11685) [quant-ph], (2019)
55. R. Jozsa, Fidelity for mixed quantum states. *J. Mod. Opt.* **41**, 2315–2323 (1994). doi: [10.1080/09500349414552171](https://doi.org/10.1080/09500349414552171)
56. Y. Aharonov, D. Z. Albert, L. Vaidman, How the result of a measurement of a component of the spin of a spin-1/2 particle can turn out to be 100. *Phys. Rev. Lett.* **60**, 1351–1354 (1988). doi: [10.1103/PhysRevLett.60.1351](https://doi.org/10.1103/PhysRevLett.60.1351); pmid: [10038016](https://pubmed.ncbi.nlm.nih.gov/10038016/)
57. G. Mitchison, R. Jozsa, S. Popescu, Sequential weak measurement. *Phys. Rev. A* **76**, 062105 (2007). doi: [10.1103/PhysRevA.76.062105](https://doi.org/10.1103/PhysRevA.76.062105)
58. A. Feizpour, X. Xing, A. M. Steinberg, Amplifying single-photon nonlinearity using weak measurements. *Phys. Rev. Lett.* **107**, 133603 (2011). doi: [10.1103/PhysRevLett.107.133603](https://doi.org/10.1103/PhysRevLett.107.133603); pmid: [22026853](https://pubmed.ncbi.nlm.nih.gov/22026853/)
59. M. Berry, P. Shukla, Pointer supershifts and superoscillations in weak measurements. *J. Phys. A Math. Theor.* **45**, 15301–15315 (2012). doi: [10.1088/1751-8113/45/1/015301](https://doi.org/10.1088/1751-8113/45/1/015301)
60. B. Tamir, E. Cohen, Introduction to weak measurements and weak values. *Quantum* **2**, 7–17 (2013). doi: [10.12743/quantum.v2i14](https://doi.org/10.12743/quantum.v2i14)
61. S. J. Smith, E. M. Purcell, Visible light from localized surface charges moving across a grating. *Phys. Rev.* **92**, 1069 (1953). doi: [10.1103/PhysRev.92.1069](https://doi.org/10.1103/PhysRev.92.1069)
62. N. Talebi, Schrödinger electrons interacting with optical gratings: Quantum mechanical study of the inverse Smith-Purcell effect. *New J. Phys.* **18**, 123006 (2016). doi: [10.1088/1367-2630/18/12/123006](https://doi.org/10.1088/1367-2630/18/12/123006)
63. A. Gover, Y. Pan, Dimension-dependent stimulated radiative interaction of a single electron quantum wavepacket. *Phys. Lett. A* **382**, 1550–1555 (2018). doi: [10.1016/j.physleta.2018.03.049](https://doi.org/10.1016/j.physleta.2018.03.049)
64. Y. Pan, A. Gover, Spontaneous and stimulated emissions of a preformed quantum free-electron wave function. *Phys. Rev. A* **99**, 052107 (2019). doi: [10.1103/PhysRevA.99.052107](https://doi.org/10.1103/PhysRevA.99.052107)
65. V. di Giulio, F. J. García de Abajo, Free-electron shaping using quantum light. *Optica* **7**, 1820–1830 (2020). doi: [10.1364/OPTICA.404598](https://doi.org/10.1364/OPTICA.404598)
66. A. Ben Hayun *et al.*, Shaping quantum photonic states using free electrons. *Sci. Adv.* **7**, eabe4270 (2021). doi: [10.1126/sciadv.abe4270](https://doi.org/10.1126/sciadv.abe4270); pmid: [33692108](https://pubmed.ncbi.nlm.nih.gov/33692108/)
67. F. J. García de Abajo, V. di Giulio, Optical excitations with electron beams: Challenges and opportunities. *ACS Photonics* **8**, 945–974 (2021). doi: [10.1021/acsp Photonics.0c01950](https://doi.org/10.1021/acsp Photonics.0c01950)
68. A. Karnieli, N. Rivera, A. Arie, I. Kaminer, Superradiance and subradiance due to quantum interference of entangled free electrons. *Phys. Rev. Lett.* **127**, 060403 (2021). doi: [10.1103/PhysRevLett.127.060403](https://doi.org/10.1103/PhysRevLett.127.060403)
69. C. Mechel *et al.*, Quantum correlations in electron microscopy. *Optica* **8**, 70 (2021). doi: [10.1364/OPTICA.402693](https://doi.org/10.1364/OPTICA.402693)
70. O. Kfir, V. Di Giulio, F. J. G. de Abajo, C. Ropers, Optical coherence transfer mediated by free electrons. *Sci. Adv.* **7**, eabf6380 (2021). doi: [10.1126/sciadv.abf6380](https://doi.org/10.1126/sciadv.abf6380); pmid: [33931451](https://pubmed.ncbi.nlm.nih.gov/33931451/)
71. A. Karnieli, N. Rivera, A. Arie, I. Kaminer, The coherence of light is fundamentally tied to the quantum coherence of the emitting particle. *Sci. Adv.* **7**, eabf8096 (2021). doi: [10.1126/sciadv.abf8096](https://doi.org/10.1126/sciadv.abf8096); pmid: [33931454](https://pubmed.ncbi.nlm.nih.gov/33931454/)
72. R. Marchetti, C. Lacava, L. Carroll, K. Gradkowski, P. Minzioni, Coupling strategies for silicon photonics integrated chips. *Photon. Res.* **7**, 201 (2019). doi: [10.1364/PRJ.7.000201](https://doi.org/10.1364/PRJ.7.000201)
73. K. J. Leedle *et al.*, Dielectric laser acceleration of sub-100 keV electrons with silicon dual-pillar grating structures. *Opt. Lett.* **40**, 4344–4347 (2015). doi: [10.1364/OL.40.004344](https://doi.org/10.1364/OL.40.004344); pmid: [26371932](https://pubmed.ncbi.nlm.nih.gov/26371932/)
74. M. Uchida, A. Tonomura, Generation of electron beams carrying orbital angular momentum. *Nature* **464**, 737–739 (2010). doi: [10.1038/nature08904](https://doi.org/10.1038/nature08904); pmid: [20360737](https://pubmed.ncbi.nlm.nih.gov/20360737/)
75. J. Verbeeck, H. Tian, P. Schattschneider, Production and application of electron vortex beams. *Nature* **467**, 301–304 (2010). doi: [10.1038/nature09366](https://doi.org/10.1038/nature09366); pmid: [20844532](https://pubmed.ncbi.nlm.nih.gov/20844532/)
76. B. J. McMorrán *et al.*, Electron vortex beams with high quanta of orbital angular momentum. *Science* **331**, 192–195 (2011). doi: [10.1126/science.1198804](https://doi.org/10.1126/science.1198804); pmid: [21233382](https://pubmed.ncbi.nlm.nih.gov/21233382/)
77. N. Voloch-Bloch, Y. Lereah, Y. Lilach, A. Gover, A. Arie, Generation of electron Airy beams. *Nature* **494**, 337–335 (2013). doi: [10.1038/nature11840](https://doi.org/10.1038/nature11840); pmid: [23426323](https://pubmed.ncbi.nlm.nih.gov/23426323/)
78. K. Y. Bliokh *et al.*, Theory and applications of free-electron vortex states. *Phys. Rep.* **690**, 1–70 (2017). doi: [10.1016/j.physrep.2017.05.006](https://doi.org/10.1016/j.physrep.2017.05.006)
79. R. Shiloh *et al.*, Spherical aberration correction in a scanning transmission electron microscope using a sculpted thin film. *Ultramicroscopy* **189**, 46–53 (2018). doi: [10.1016/j.ultramicro.2018.03.016](https://doi.org/10.1016/j.ultramicro.2018.03.016); pmid: [29614394](https://pubmed.ncbi.nlm.nih.gov/29614394/)
80. O. Reinhardt, I. Kaminer, Theory of Shaping Electron Wavepackets with Light. *ACS Photonics* **7**, 2859–2870 (2020). doi: [10.1021/acsp Photonics.0c01133](https://doi.org/10.1021/acsp Photonics.0c01133)
81. G. M. Vanacore, I. Madan, F. Carbone, Spatio-temporal shaping of a free-electron wave function via coherent light–electron interaction. *Riv. Nuovo Cim.* **43**, 567–597 (2020). doi: [10.1007/s40766-020-00012-5](https://doi.org/10.1007/s40766-020-00012-5)
82. A. Gover, A. Yarif, Free-electron-bound-electron resonant interaction. *Phys. Rev. Lett.* **124**, 064801 (2020). doi: [10.1103/PhysRevLett.124.064801](https://doi.org/10.1103/PhysRevLett.124.064801); pmid: [32109105](https://pubmed.ncbi.nlm.nih.gov/32109105/)
83. S. Tsesses *et al.*, Spatial modulation of free-electron wavepackets by shaping ultrafast plasmonic excitations. *CLEO Conference FTu3B.4* (2020).
84. M. Kozák, N. Schönenberger, P. Hommelhoff, Ponderomotive generation and detection of attosecond free-electron pulse trains. *Phys. Rev. Lett.* **120**, 103203 (2018). doi: [10.1103/PhysRevLett.120.103203](https://doi.org/10.1103/PhysRevLett.120.103203); pmid: [29570333](https://pubmed.ncbi.nlm.nih.gov/29570333/)
85. J.-W. Henke, A. S. Raja, A. Feist, G. Huang, G. Arend, Y. Yang, J. Kappert, R. N. Wang, M. Möller, J. Pan, J. Liu, O. Kfir, C. Ropers, T. J. Kippenberg, Integrated photonics enables continuous-beam electron phase modulation. [arXiv:2105.03729](https://arxiv.org/abs/2105.03729) [physics.optics] (2021).
86. B. W. Shore, P. L. Knight, The Jaynes-Cummings model. *J. Mod. Opt.* **40**, 1195–1238 (1993). doi: [10.1080/09500349314551321](https://doi.org/10.1080/09500349314551321)

ACKNOWLEDGMENTS

We thank E. Cohen for the fruitful discussions regarding the classical/quantum walk description. We also thank IDES and especially S. T. Park for support, advice, and discussions. We thank T. Gondo and H. Miyazaki (Mel-Build Corporation) for the specially designed HATA-holder. The experiments were performed on the UTEM of the AdQuanta group of I.K., which is installed inside the electron microscopy center (MIKA) of the Department of Materials Science and Engineering at the Technion. We thank the MPL cleanroom staff for continued technical support. I.K., M.S., and their students gratefully acknowledge the generous support of R. Magid and R. Magid, who have made it possible to carry out these experiment at the UTEM lab at the Technion. **Funding:** This project has received funding from the European Union's Horizon 2020 research and innovation program under grant agreement 851780-ERC-NanoEP, the Israel Science Foundation (grant 830/19), the Binational USA-Israel Science Foundation (BSF) 2018288, Gordon and Betty Moore Foundation grant 4744 (ACHIP), and ERC Advanced Grant 884217 (AccelOnChip). A.K. acknowledges support by the Adams Fellowship of the Israeli Academy of Sciences and Humanities. **Author contributions:** All authors contributed substantially to this work. **Competing interests:** None declared. **Data and materials availability:** All data needed to evaluate the conclusions in the paper are present in the paper or the supplementary materials.

SUPPLEMENTARY MATERIALS

<https://science.org/doi/10.1126/science.abj7128>
Materials and Methods
Supplementary Text
Figs. S1 to S17
References (87–97)

27 May 2021; accepted 9 August 2021
Published online 26 August 2021
[10.1126/science.abj7128](https://doi.org/10.1126/science.abj7128)

Imprinting the quantum statistics of photons on free electrons

Raphael DahanAlexey Gorklachs Urs HaeuslerAviv KarnieliOri EyalPeyman YousefiMordechai SegevAdy ArieGadi EisensteinPeter HommelhoffIldo Kaminer

Science, 373 (6561), eabj7128. • DOI: 10.1126/science.abj7128

Electrons see the quantum nature of light

We know that light is both a wave and a particle, and this duality arises from the classical and quantum nature of electromagnetic excitations. Dahan *et al.* observed that all experiments to date in which light interacts with free electrons have been described with light considered as a wave (see the Perspective by Carbone). The authors present experimental evidence revealing the quantum nature of the interaction between photons and free electrons. They combine an ultrafast transmission electron microscope with a silicon-photonics nanostructure that confines and strengthens the interaction between the light and the electrons. The “quantum” statistics of the photons are imprints onto the propagating electrons and are seen directly in their energy spectrum. —ISO

View the article online

<https://www.science.org/doi/10.1126/science.abj7128>

Permissions

<https://www.science.org/help/reprints-and-permissions>

Use of this article is subject to the [Terms of service](#)

Science (ISSN) is published by the American Association for the Advancement of Science. 1200 New York Avenue NW, Washington, DC 20005. The title *Science* is a registered trademark of AAAS.

Copyright © 2021 The Authors, some rights reserved; exclusive licensee American Association for the Advancement of Science. No claim to original U.S. Government Works